

Surface tension of liquid Al–Cu–Ag ternary alloys

J. Brillo · Y. Plevachuk · I. Egry

Received: 17 February 2010/Accepted: 9 April 2010/Published online: 22 April 2010
© Springer Science+Business Media, LLC 2010

Abstract Surface tension data of liquid Al–Cu–Ag ternary alloys have been measured contactlessly using the technique of electromagnetic levitation. A digital CMOS-camera (400 fps) recorded image sequences of the oscillating liquid sample and the surface tension was determined from an analysis of the frequency spectra. Data were obtained at temperatures above the melting point. Samples covered a broad range of compositions. In all cases, the surface tensions could be described as linear functions of temperature with a negative slope. The data were compared to thermodynamic model calculations using the ideal- and subregular solution approximation. It was found that, apart from samples where the composition is close to one of the binary margin phases, the surface tensions of the ternary alloys can be described by the ideal solution model.

Introduction

The Al–Cu–Ag ternary alloy system is important for mainly two reasons: First, it serves as a model to study ternary eutectic alloys [1, 2]; and second, it appears in a number of technical applications. The most prominent of them is high temperature soldering of Al with Ag–Cu where, at the interface, a ternary eutectic alloy forms [3].

In these examples, the key dynamic processes go hand-in-hand with surface- and interface phenomena [4]. The

involved thermophysical properties, in particular, interfacial energies and surface tension, need to be known precisely.

Measurements of the bulk properties density and viscosity, carried out recently on this system [5], indicate that Al–Cu–Ag is highly non-ideal with respect to these properties. The same was found for the density of the binary systems Al–Cu and Al–Ag [6], as well as for the surface tension of liquid Al–Cu alloys [7]. Surface tension data of pure silver have been reported recently [8, 9].

This study focusses on the measurement of surface tension data of liquid Al–Cu–Ag alloys covering a broad range of compositions. It is likely that, with respect to surface tension, Al–Cu–Ag will behave highly non-ideal as well. In order to check this hypothesis and, to be able to interpolate the results throughout the entire ternary system, the obtained surface tension data will be compared to ideal and non-ideal solution models using the Butler equation [10–12].

The Butler equation is based on the assumption that the surface of the liquid is a monolayer of atoms. This monolayer is regarded as an individual thermodynamic phase which is in equilibrium with the bulk.

When i denotes one of the three elements of the ternary alloy ($i = \text{Al}, \text{Cu}, \text{Ag}$), $\gamma_i(T)$ the corresponding surface tensions at temperature, T , c_i^B the concentration of element i in the bulk phase, and c_i^S the corresponding concentration in the surface phase, the Butler equation is given by the following expression:

$$\gamma_{\text{AlCuAg}}(T) = \gamma_i + \frac{RT}{S_i} \ln \left(\frac{c_i^S}{c_i^B} \right) + \frac{1}{S_i} \{ {}^E G_i^S(T, c_i^S) - {}^E G_i^B(T, c_i^B) \} \quad (1)$$

here, R is the universal gas constant, ${}^E G_i^B$ and ${}^E G_i^S$ denote the respective partial excess Gibbs energies of component i

J. Brillo (✉) · I. Egry
Institut für Materialphysik im Weltraum, Deutsches Zentrum
für Luft- und Raumfahrt (DLR), 51170 Köln, Germany
e-mail: Juergen.Brillo@dlr.de

Y. Plevachuk
Department of Metal Physics, Ivan Franko National University,
Lviv 79005, Ukraine

in the bulk and in the surface layer, and S_i is the molar surface area of pure liquid i . It is calculated from the molar volume of the pure element, V_i , according to following equation:

$$S_i(T) = f \cdot V_i^{2/3} N_{\text{Av}}^{1/3} \quad (2)$$

Here, N_{Av} is the Avogadro number and f is a geometrical factor which is taken as 1.09 [13, 14]. This value corresponds to an assumed atomic arrangement in the surface similar to an fcc (111) plane with a coordination number in the bulk of $z \approx 12$. This value for z was confirmed by recent studies, performed with X-ray and neutron scattering as well as by molecular dynamics simulations. It is a good estimate at least for Cu, Fe, Ni, Co, and Al–(Co, Ni, Fe) binary alloys [15–17]. A value of $f = 1.06$, based on a coordination number of $z = 11$, was suggested recently [13]. Within the experimental error, the difference using the above value of $f = 1.09$ is negligible.

The main assumption of the Butler model is the approximation of the surface excess Gibbs energy, ${}^E G^S(T, c_i^S)$, by [18]:

$${}^E G^S(T, c_i^S) \approx \xi \cdot {}^E G^B(T, c_i^S) \quad (3)$$

The phenomenological factor ξ accounts in a crude way for the reduced coordination in the surface layer. It can be thought of as the ratio of the respective coordination numbers of atoms in the surface and in the bulk. Surface ordering effects as well as a possibly existing dependence of ξ on composition are not included. Depending on the atomic short-range order in the liquid, ξ varies from 0.5 to 1 [14, 18–20]. A constant value of 0.75 was initially suggested by Tanaka and Iida [14] as a default approximation for liquids with unknown structure. Later, they replaced this value by 0.83 which was also used in this study [20].

In Eq. 3, the partial excess energy ${}^E G_i^B$ is derived from the excess energy ${}^E G$ using the following set of equations [14]:

$$\begin{aligned} {}^E G_{\text{Al}}^B(T, c_{\text{Cu}}^B, c_{\text{Ag}}^B) &= {}^E G - c_{\text{Cu}}^B \frac{\partial {}^E G}{\partial c_{\text{Cu}}^B} - c_{\text{Ag}}^B \frac{\partial {}^E G}{\partial c_{\text{Ag}}^B} \\ {}^E G_{\text{Cu}}^B(T, c_{\text{Cu}}^B, c_{\text{Ag}}^B) &= {}^E G + (1 - c_{\text{Cu}}^B) \frac{\partial {}^E G}{\partial c_{\text{Cu}}^B} - c_{\text{Ag}}^B \frac{\partial {}^E G}{\partial c_{\text{Ag}}^B} \\ {}^E G_{\text{Ag}}^B(T, c_{\text{Cu}}^B, c_{\text{Ag}}^B) &= {}^E G - c_{\text{Cu}}^B \frac{\partial {}^E G}{\partial c_{\text{Cu}}^B} + (1 - c_{\text{Ag}}^B) \frac{\partial {}^E G}{\partial c_{\text{Ag}}^B} \end{aligned} \quad (4)$$

The excess energy ${}^E G^B$ is usually written in the following form [14, 19, 21]:

$${}^E G^B(c_1^B, \dots, c_3^B, T) = \sum_i^2 \sum_{j>i}^3 c_i^B c_j^B {}^E G_{i,j}^B \quad (5)$$

The parameter ${}^E G_{i,j}$ describes the binary interaction between two components i and j . It can be written as

a function of temperature, T , and concentration, c_i^B , according to the Redlich–Kister form [21, 22]:

$${}^E G_{i,j} = \sum_{v=0} {}^v L_{i,j}(T)(c_i^B - c_j^B)^v \quad (6)$$

In Eq. 6, the coefficients ${}^v L_{i,j}(T)$ depend on temperature but not on the concentrations. Generally, there is also a parameter for a ternary interaction which, in the case of Al–Cu–Ag, is not taken into account [12, 23, 24].

Details of the solution of the Butler equation are also described in Refs. [11, 12, 25].

Experimental

Electromagnetic levitation

Surface tension measurements are very sensitive to the purity conditions of the sample material. In standard container-based techniques, reactions between the liquid specimen and the container must be carefully avoided [26]. The technique of electromagnetic levitation [27] allows contactless investigations and provides high-purity conditions necessary for surface tension measurements and is used in this study. As an alternative, Paradis et al. [28] employed electrostatic levitation.

Electromagnetic levitation experiments were performed in a standard stainless steel high vacuum chamber filled with 600-mbar He after prior evacuation. The samples had a typical diameter of 4 mm and were positioned in the centre of a levitation coil. The inhomogeneous electromagnetic field induces eddy currents inside the sample so that it can be positioned stably against gravity. Due to ohmic losses the sample is heated and molten. In order to adjust a certain desired temperature, it is cooled in a laminar flow of the He gas provided by an alumina nozzle underneath. Temperature was measured by a pyrometer focussed at the sample from the side. As the emissivity is generally not known, the pyrometer output signal, T_P , was recalibrated with respect to the liquidus temperature T_L . This is done under the assumption that within the operating wavelength range of the pyrometer the emissivity of the specimen material does not change with temperature. This is a good approximation for most liquid metals [29]. T is determined from the following expression derived from Wien's law:

$$\frac{1}{T} - \frac{1}{T_P} = \frac{1}{T_L} - \frac{1}{T_{L,P}} \quad (7)$$

Here, $T_{L,P}$ denotes the pyrometer signal at liquidus temperature. It is identified by a kink in T_P at the time when the melting process is completed and the temperature starts to rise with a steeper slope [30].

Table 1 Parameters T_L , γ_L , and γ_T of each of the investigated alloys. The table also shows the interpolated surface tension at 1000 °C

Alloy	T_L (°C)	γ_L (N/m)	γ_T (10^{-4} Nm $^{-1}$ K $^{-1}$)	γ ($T = 1000$ °C)
Cu ₉₀ Ag ₁₀	1009	1.15	-2.2	1.15
Al ₂₀ Cu ₇₀ Ag ₁₀	972	1.06	-4.5	1.06
Al ₄₀ Cu ₅₀ Ag ₁₀	861	1.01	-2.1	0.99
Al ₅₀ Cu ₄₀ Ag ₁₀	736	1.01	-3.9	0.91
Al ₇₀ Cu ₂₀ Ag ₁₀	545	1.05	-3.7	0.89
Al ₉₀ Ag ₁₀	628	0.95	-2.7	0.85
Al ₁₇ Cu ₈₃	1044	1.32	-2.7	1.33
Al ₅₅ Cu ₁₅ Ag ₃₀	591	0.90	-1.0	0.92
Al ₄₀ Cu ₁₀ Ag ₅₀	688	0.97	-2.9	1.08
Al ₃₅ Cu ₃₅ Ag ₃₀	771	1.01	-2.5	1.15
Al ₄₀ Cu ₆₀	955	1.13	-1.54	1.12

In this study, values for T_L were obtained from CALPHAD [22] calculations performed and communicated by R. Schmid-Fetzer, TU Clausthal, see Table 1.

Oscillating drop method

The surface tension, γ , is determined by means of the oscillating drop method [31]. This technique is based on the fact that surface tension acts as a restoring force for the oscillations of a liquid droplet. Their frequencies thus serve as a direct measure of γ .

In electromagnetic levitation, the sample shape is elongated slightly in the vertical direction and the $l = 2$ Rayleigh mode splits up into a set of five frequencies ω_m with $m = -2, -1, 0, 1, 2$. Per temperature step, they are measured by recording 4,096 images of the oscillating drop using a high-resolution C-MOS camera with 400 fps. This takes approximately 50 s including the time for saving the images.

The subsequent analysis with an edge detection algorithm produces frequency spectra as shown in Fig. 1. They are Fourier transforms of the difference and the sum signal of two perpendicular radii. Using a symmetry rule, the peaks at ω_m , marked by arrows in Fig. 1, can be identified [31]. The surface tension, γ , is calculated from these frequencies using the formula of Cummings and Blackburn [32]:

$$\gamma = \frac{3M}{160\pi} \sum_{m=-2}^2 \omega_m^2 - 1.9\Omega^2 - 0.3 \left(\frac{g}{a} \right)^2 \Omega^{-2} \quad (8)$$

Here M is the mass of the sample, a its radius, and g is the gravitational acceleration. In Eq. 8, the parameter Ω corrects for the magnetic pressure. It is calculated from the three translational frequencies, $\omega_{x,y,z}$, corresponding to the horizontal and vertical movements of the sample: $\Omega^2 = 1/3(\omega_x^2 + \omega_y^2 + \omega_z^2)$. Depending on the mass of the sample,

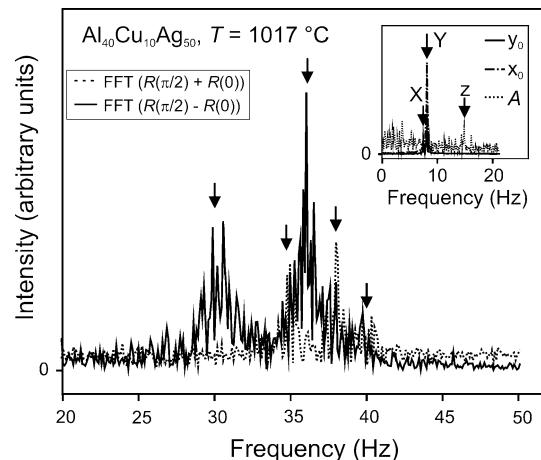


Fig. 1 Typical frequency spectra of the surface oscillations of a liquid Al₄₀Cu₁₀Ag₅₀ sample at $T = 1017$ °C. Solid curve Fourier transform of the difference signal of two perpendicular radii. Dotted curve Fourier transform of the sum signal of two perpendicular radii. The inset shows Fourier transforms of the x (dash-dotted) and y (solid line) coordinate of the centre of mass as well as of the apparent sample area (dotted line). The arrows mark the frequencies of the three translations in X -, Y -, and Z -direction

the frequencies of the translational movements are typically between 5 and 20 Hz, where as a rule of thumb, $\omega_Z \approx 2\omega_X \approx 2\omega_Y$. The frequencies ω_X and ω_Y are determined from the horizontal movement of the droplet centre, while ω_Z is extracted from the spectrum of the apparent droplet area.

The relative error of the surface tension is approximately $\Delta\gamma/\gamma \approx 5\%$ [7].

Sample selection and preparation

The compositions of the investigated samples are listed in Table 1. As shown in Fig. 2, three sections through the ternary system, denoted as “A”, “B”, and “C” were investigated. The local environment of these sections include the ternary eutectic point (Al_{69.1}Cu_{12.8}Ag_{18.1}) located in the aluminium-rich corner of the ternary phase diagram.

In Section A the concentrations of Al and Cu were changed, while the concentration of Ag was kept constant at 10 at.%. Hence, Section A can be summarized by the sum formula Al_xCu_{90-x}Ag₁₀.

In Section B, the silver concentration is the main parameter and ranges from 0 to 100 at.%, while the ratio of the Al concentration to the copper concentration is constant, $c_{\text{Al}}^{\text{B}}/c_{\text{Cu}}^{\text{B}} = 77:23$. Thus, Section B is described by Al_{0.77(100-x)}Cu_{0.23(100-x)}Ag_x.

Finally, in Section C, the Al concentration is kept constant at 40 at.%, while the concentrations of Cu and Ag are changed according to the sum formula Al₄₀Cu_{60-x}Ag_x.

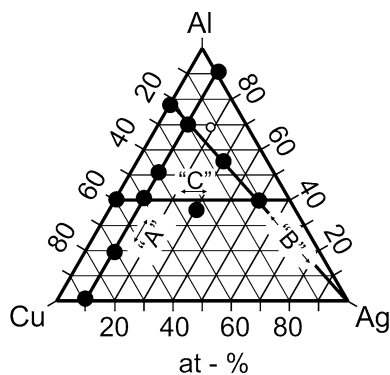


Fig. 2 Concentrations of the investigated samples. Along Section A, the silver concentration is kept constant at $c_{\text{Ag}}^{\text{B}} = 10\%$, while the Al concentration is varied. Along Section B, the concentration of silver is the main parameter and the ratio of $c_{\text{Al}}^{\text{B}}:c_{\text{Cu}}^{\text{B}}$ is approximately 77:23. The concentration of Al is kept at 40 at.%, while the Ag concentration is varied along Section C. The hollow circle marks the position of the ternary eutectic point

Samples with corresponding Al, Cu, and Ag concentrations were prepared by melting together the required amounts of the constituent elements in an arc furnace.

In order to obtain a homogeneous alloy, each sample was shortly melted in a levitation process prior to the actual experiment. In this step, the temperature was raised for a few seconds up to 1700 °C. Traces of Al oxide, which possibly existed on the surface, decomposed this way and evaporated so that an additional cleaning of the sample was achieved.

Results

Measurements were performed over a temperature range of typically $850 \text{ }^{\circ}\text{C} \leq T \leq 1200 \text{ }^{\circ}\text{C}$. Due to the high vapour pressure of silver, the temperature was limited to a maximum of 1200 °C. At temperatures lower than approximately 850 °C the samples appeared too dark for the used C-MOS camera. Moreover, undercooling could not be achieved. All investigated specimen exhibit a linear dependence of the surface tension on temperature with a negative slope. This is shown in Fig. 3 for the example of Section A.

As visible, the relative error, i.e. the scatter in the data, is less than approximately $\pm 3\%$. The surface tension values can be represented by the following linear function with fit parameters γ_L and γ_T describing the surface tension at T_L and its temperature coefficient:

$$\gamma = \gamma_L + \gamma_T(T - T_L) \quad (9)$$

These parameters are listed in Table 1 for all investigated samples. They are used to study the concentration dependence from interpolating the surface tension by Eq. 9 to $T = 1000 \text{ }^{\circ}\text{C}$. This temperature was chosen because it lies

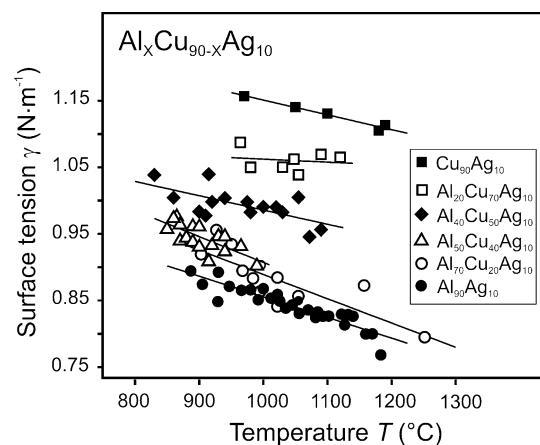


Fig. 3 Measured surface tensions, γ , of liquid Al–Cu–Ag samples of Section A versus temperature. The straight lines correspond to linear fits

almost in the centre of the temperature range investigated of all the samples.

The results for Sections A, B, and C are shown in Figs. 4, 5, and 6, respectively.

In Fig. 4, γ is plotted versus Al concentration, c_{Al}^{B} . The experimental points are located along a concave curve. The surface tension decreases monotonically with increasing c_{Al}^{B} from approximately 1.2 N/m, which corresponds to $\text{Cu}_{90}\text{Ag}_{10}$, down to 0.85 N/m for $\text{Al}_{90}\text{Ag}_{10}$.

A practically constant course of γ versus c_{Ag}^{B} is found along Section B in Fig. 5. Here, $\gamma \approx 0.87 \text{ N/m}$. Alloys with more than 50 at.% Ag could not be measured due to pronounced evaporation of silver that occurred in these alloys during processing.

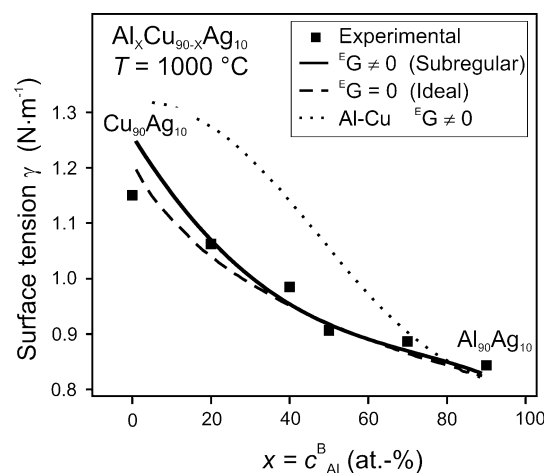


Fig. 4 Surface tension values of Al–Cu–Ag samples of Section A at 1000 °C versus Al bulk concentration. The data are shown in comparison with solutions of the Butler equation for the ideal (dashed line) and the subregular solution model (solid line). The dotted line corresponds to a calculation of the subregular solution model for Al–Cu

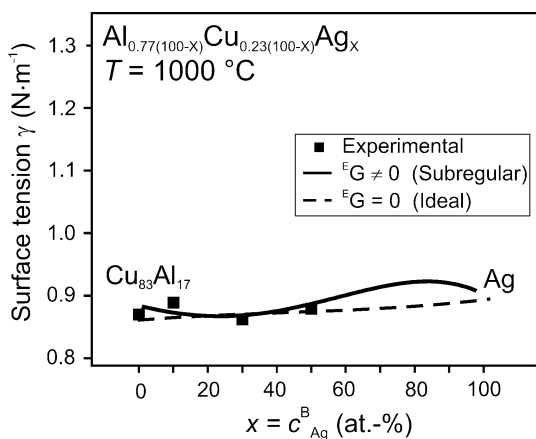


Fig. 5 Surface tension values of Al–Cu–Ag samples of Section B at 1000 °C versus Ag bulk concentration. The data are shown in comparison with solutions of the Butler equation for the ideal (dashed line) and the subregular solution model (solid line)

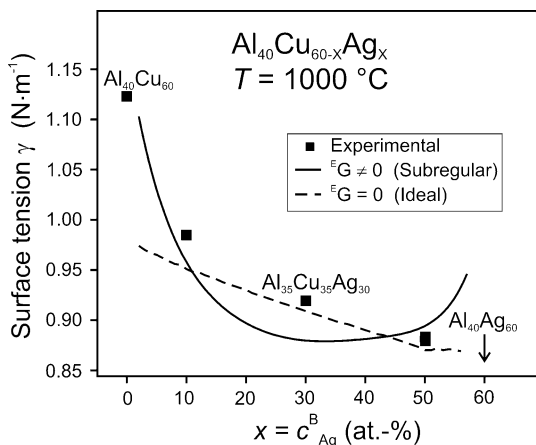


Fig. 6 Surface tension values of Al–Cu–Ag samples of Section C at 1000 °C versus Ag bulk concentration. The data are shown in comparison with solutions of the Butler equation for the ideal (dashed line) and the subregular solution model (solid line)

Essentially the same picture as in Fig. 4 is provided by Fig. 6. Here, γ is shown as function of the silver concentration, c_{Ag}^{B} , along Section C. It decreases with increasing c_{Ag}^{B} from approximately 1.15 N/m, for binary $\text{Al}_{40}\text{Cu}_{60}$, to 0.9 N/m for $\text{Al}_{40}\text{Ag}_{60}$. The steepest decrease of the surface tension takes place in the region where $c_{\text{Ag}}^{\text{B}} < 10$ at.%. Hence, the dependence of the surface tension on concentration is slightly stronger for Section C than for Section A in Fig. 4.

Discussion

The experimental data in Figs. 4, 5, and 6 are compared to calculations of the Butler equation for the ideal, ${}^{\text{E}}G^{\text{B}} = 0$,

and the subregular solution model, ${}^{\text{E}}G^{\text{B}} \neq 0$. Input parameters for the Butler equation, density and surface tension of the pure components, are listed in Table 2.

Parameters of the surface tension of pure silver from various references are compiled in Table 3. The values agree within $\pm 5\%$ with each other. The parameters given by Ref. [8] are slightly larger than the others. This is attributed by the authors to the controlled experimental conditions using electromagnetic levitation. In order to keep the results consistent with our previous works, we decided to use values for γ_{Ag} from Ref. [9].

For the subregular solution model, Eqs. 5 and 6 are applied. The coefficients ${}^v G_{i,j}(T)$ needed in Eq. 6 have been reported by Witusiewicz [33, 34] up to fourth order, $v = 4$. They are listed in Table 4.

In Figs. 4 and 5, a good agreement between the experimental data and the calculations is found for both, the ideal and the subregular solution model. The surface tensions predicted by the subregular solution model are slightly larger than the ones predicted by the ideal solution but, with respect to the relative uncertainty in the measurements, $\Delta\gamma/\gamma \approx 5\%$, both models describe the experimental data equally well.

A reasonably good agreement with the measured data is also found for the subregular solution model in Fig. 6. In particular, it reproduces the strong increase of the surface tension with decreasing c_{Ag}^{B} in the range of $c_{\text{Ag}}^{\text{B}} < 10$ at.%. In this concentration range, the ternary system approximates its binary margin, Al–Cu, and the observed behaviour mirrors the already known fact that Al–Cu is generally a highly non-ideal system [6, 7].

A remarkable deviation between the calculation for the subregular solution and the experimental data is evident for the single data point at $c_{\text{Ag}}^{\text{B}} = 30$ at.%. Here, the experimentally obtained surface tension is approximately 5–6% larger. This deviation is due to the fact that the composition of the corresponding ternary alloy, $\text{Al}_{35}\text{Cu}_{35}\text{Ag}_{30}$, is slightly off the line of Section C in Fig. 2.

In Fig. 6, the ideal solution model yields an almost straight line with a negative slope. Like it was found already for Sections A and B (Figs. 4, 5, respectively), both the models describe the data equally well with respect to the experimental error. The ideal solution model fails, however, at low silver concentrations, i.e. in the limit of the binary system. This is already evident from the comparison of the results of Section A with the binary Al–Cu system, see Fig. 4. Here, the dotted line represents a calculation of the subregular solution model which, as discussed in Ref. [7], describes the experimental data of Al–Cu. It significantly deviates from the results for the ternary Al–Cu–Ag. Hence, with respect to surface tension, an addition of only 10 at.% of silver to Al–Cu is sufficient to make the highly non-ideal system ideal.

Table 2 Parameters entering the Butler equation: surface tension, γ_L , and density, ρ_L , of the pure components at liquidus, T_L , and their respective temperature coefficients, γ_T and ρ_T

Element	T_L (°C)	γ_L (N/m)	ρ_L (g/cm ³)	γ_T (10 ⁻⁴ Nm ⁻¹ K ⁻¹)	ρ_T (10 ⁻⁴ g cm ⁻³ K ⁻¹)	References
Al	660	0.87	2.35	-1.6	-2.0	[6, 35]
Cu	1085	1.30	7.92	-2.6	-7.6	[6, 7]
Ag	960	0.91	9.15	-1.8	-7.4	[6, 9]

Table 3 Compilation of surface tension values, γ_L and γ_T , for liquid silver

γ_L (N m ⁻¹)	γ_T (10 ⁻⁴ N m ⁻¹ K ⁻¹)	References
0.966	-2.5	[8]
0.91	-1.8	[9]
0.925	-2.1	[36, 37]
0.916	-2.28	[38]

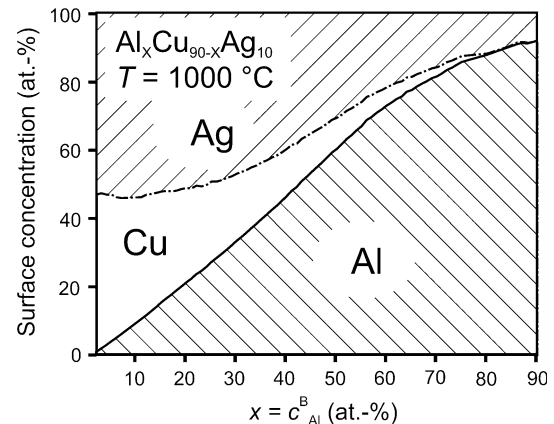
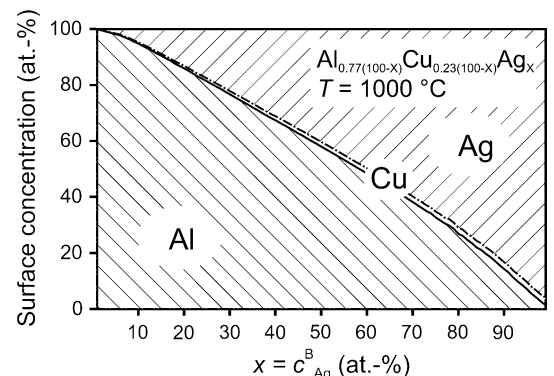
Table 4 Redlich–Kister coefficients $L_{i,j}$ used to calculate the excess Gibbs energy E_G^B according to Eqs. 5 and 6, from Refs. [33, 34]

Parameter	Value (J mol ⁻¹)
${}^0L_{\text{Al},\text{Cu}}$	$-67094 + 8.555T$
${}^1L_{\text{Al},\text{Cu}}$	$32148 - 7.118T$
${}^2L_{\text{Al},\text{Cu}}$	$5915 - 5.889T$
${}^3L_{\text{Al},\text{Cu}}$	$-8175 + 6.049T$
${}^0L_{\text{Ag},\text{Al}}$	$-15022 - 20.538T$
${}^1L_{\text{Ag},\text{Al}}$	$-20456 - 17.291T$
${}^2L_{\text{Ag},\text{Al}}$	$-3821 - 17.17T$
${}^3L_{\text{Ag},\text{Al}}$	$7028 - 12.247T$
${}^4L_{\text{Ag},\text{Al}}$	$7661 - 5.857T$
${}^1L_{\text{Ag},\text{Cu}}$	$14463 - 1.516T$
${}^2L_{\text{Ag},\text{Cu}}$	$-934 - 0.319T$

In summary, the surface tension of the Al–Cu–Ag ternary system can be described by the ideal solution model, as long as the composition is not located at the margin of the system, i.e. close to one of the binary phases.

In order to understand this unexpected finding, the chemical composition of the surface layer, as obtained from the Butler equation, needs to be discussed. This is done for the three sections in Figs. 7, 8, and 9.

In Fig. 7, the surface concentrations c_{Al}^S , c_{Cu}^S , and c_{Ag}^S are depicted as a function of c_{Al}^B . At low aluminium concentrations, $c_{\text{Al}}^B < 30$ at.%, silver is the main component in the surface with $c_{\text{Ag}}^S \leq 60$ at.%. With an increase of c_{Al}^B the Al surface concentration increases linearly with a slope larger than one, as long as $c_{\text{Al}}^B < 60$ at.%. This takes place on the expense of silver and mainly copper on the surface. Above $c_{\text{Al}}^B > 60$ at.%, the increase of c_{Al}^S with Al bulk concentration becomes slower.

**Fig. 7** Calculated surface concentrations of Al, Cu, and Ag at 1000 °C as function of Al concentration, Section A. The solid line shows c_{Al}^S and the dash-dotted line corresponds to $c_{\text{Al}}^S + c_{\text{Cu}}^S = 1 - c_{\text{Ag}}^S$ **Fig. 8** Calculated surface concentrations of Al, Cu, and Ag at 1000 °C as function of Al concentration, Section B. The solid line shows c_{Al}^S and the dash-dotted line corresponds to $c_{\text{Al}}^S + c_{\text{Cu}}^S = 1 - c_{\text{Ag}}^S$

In Figs. 8 and 9 (Sections B and C, respectively) the surface concentrations are plotted versus the silver bulk concentration c_{Ag}^B . For Section B in Fig. 8, the concentration of copper in the surface layer, c_{Cu}^S is negligible and a competitive character of the segregation of silver and aluminium is demonstrated: With increasing silver bulk concentration, c_{Ag}^S increases at the same rate at which c_{Al}^S decreases.

In Fig. 9, c_{Ag}^S increases with c_{Ag}^B on the expense of aluminium and mainly copper. The strongest increase takes place in the region where $c_{\text{Ag}}^B < 10$ at.%.

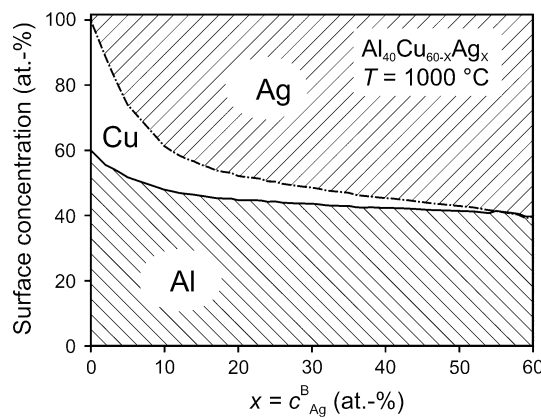


Fig. 9 Calculated surface concentrations of Al, Cu, and Ag at 1000 °C as function of Al concentration, Section C. The solid line shows c_{Al}^S and the dash-dotted line corresponds to $c_{Al}^S + c_{Cu}^S = 1 - c_{Ag}^B$

with the strong decrease of γ in the same concentration range (see Fig. 6).

The above segregation behaviour becomes plausible when it is noted that the surface tensions of silver and aluminium are of similar magnitude, $\gamma_{Ag} \approx \gamma_{Al}$, while γ_{Cu} is significantly larger. Hence, to minimise surface energy, copper is suppressed and silver and aluminium are the main chemical species at the surface.

Knowing c_{Al}^S , c_{Cu}^S , and c_{Ag}^S , it is possible to discuss the excess Gibbs energies of Al–Cu–Ag to understand why for the vast range of composition it is sufficient to describe the surface tension by means of the ideal solution model. This is performed by defining a coefficient γ^* as the ratio of the enthalpy to the ideal entropy term in the Butler equation, both taken as integral quantities to reduce the number of equations:

$$\gamma^* = \frac{\sum_i c_i^B (\bar{E}G_i^S(T, c_i^S) - \bar{E}G_i^B(T, c_i^B))}{RT \sum_i c_i^B \ln\left(\frac{c_i^S}{c_i^B}\right)} \quad (10)$$

γ^* describes the non-ideality of the system. The system is regarded as “ideal” if $\gamma^* \approx 0$. It is “non-ideal” if γ^* significantly deviates from zero. In Fig. 10, γ^* is plotted as function of silver bulk concentration along Section C. As visible, the curve is flat and close to zero, $\gamma^* \approx -0.5$, for $15 \text{ at.\%} < c_{Ag}^B < 45 \text{ at.\%}$. Hence, in this region $\bar{E}G^S(T, c_i^S) \approx \bar{E}G^B(T, c_i^B)$ so that the excess energy term cancels out in the Butler equation. In this concentration range, the surface tension can also be described by the ideal solution model.

The excess energy term does not cancel out for $c_{Ag}^B < 10 \text{ at.\%}$, i.e. near the binary margin Al–Cu. Here, γ^* significantly deviates from zero and takes on values <-3.0 . Consequently, the experimental data in this concentration range can only be described by the subregular solution approximation, as evident in Figs. 4 and 6.

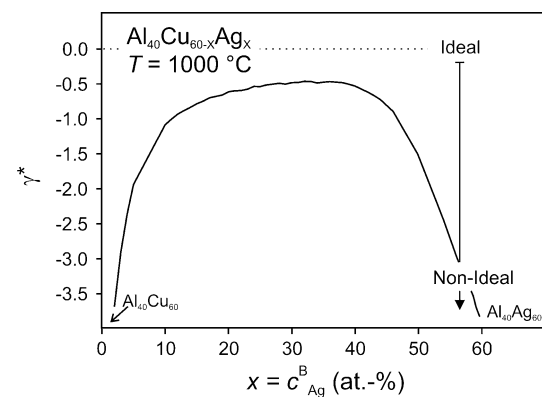


Fig. 10 Parameter γ^* as function of c_{Ag}^B along Section C. Significant deviations from zero indicate that the system is non-ideal at the corresponding concentrations

γ^* deviates significantly from zero also for $c_{Ag}^B > 45 \text{ at.\%}$. As demonstrated in Fig. 6, the surface tension can here still be described by the ideal solution model. This is due to the fact that, according to Figs. 8 and 9, the surface consists in this concentration range mainly of Al and Ag and it cannot be distinguished between the two models any longer.

Conclusions

Precise surface tension data of liquid ternary Al–Cu–Ag have been measured in a broad range of temperature and composition. A linear temperature dependence with a negative slope was observed in all cases.

The data were discussed as function of alloy composition and compared with calculations of the Butler equation for the ideal and subregular solution model.

It was found that the surface tensions of the ternary Al–Cu–Ag alloys could be described by the ideal solution model, i.e. without any knowledge of excess Gibbs energies, $\bar{E}G^B$. This holds for compositions outside the vicinity of the binary margin phases.

If the composition of the ternary alloy is close to one of the binary phases, in particular Al–Cu, the system becomes (highly) non-ideal with respect to the surface tension. Here, γ can only be described by the subregular solution model.

For the subregular solution model, the Butler equation predicts that Al and Ag are the main chemical species in the surface region, while Cu is suppressed due to its higher surface tension.

Acknowledgements The support by the “Deutsche Forschungsgemeinschaft” (Grants Eg 93/4 and 436UKR17) is gratefully acknowledged. We also wish to thank R. Schmid-Fetzer for calculating the liquidus temperatures.

References

1. Cooksey DJS, Hellawell A (1967) *J. Inst Met* 95:183
2. De Wilde J, Froyen L, Rex S (2004) *Scripta Mater* 51:533
3. Gupta P, Doraiswami R, Tumala R (2004) *Electron Compon Technol* 1:68
4. Genau A, Ratke L (2010) *Int J Mater Res* (submitted)
5. Brillo J, Brooks R, Egry I, Quested P (2008) *High Temp High Press* 37:371
6. Brillo J, Egry I, Westphal J (2008) *Int J Mater Res* 99:2
7. Schmitz J, Brillo J, Egry I, Schmid-Fetzer R (2009) *Int J Mater Res* 100:11
8. Hibiya T, Morohoshi K, Ozawa S (2010) *J Mater Sci* 45:1986. doi:[10.1007/s10853-009-4107-2](https://doi.org/10.1007/s10853-009-4107-2)
9. Egry I, Sauerland S (1994) *High Temp High Press* 26:217
10. Butler J (1935) *Proc Roy Soc A* 135:348
11. Brillo J, Chatain D, Egry I (2009) *Int J Mater Res* 100:1
12. Brillo J, Egry I, Matsushita T (2006) *Z Metallkd* 97:1
13. Kaptay G (2002) Proceedings of microcad, section: materials science, University of Miskolc, vol 45
14. Tanaka T, Iida T (1994) *Steel Res* 65:21
15. Schenk T, Holland-Moritz D, Simonet R, Bellissent R, Herlach DM (2002) *Phys Rev Lett* 89:075507
16. Schenk T, Simonet V, Holland-Moritz D, Bellissent R, Hansen T, Convert P (2004) *Europhys Lett* 65:34
17. Das SK, Horbach J, Voigtmann T (2008) *Phys. Rev. B* 78:064208
18. Hoar TP, Melford DA (1957) *Trans Farad Soc* 33:315
19. Akinlade O, Sommer F (2001) *J Alloys Compd* 316:226
20. Tanaka T, Hack K, Iida T, Hara S (1996) *Z Metallkd* 87:380
21. Lüdecke C, Lüdecke D (2000) *Thermodynamik*. Springer, Heidelberg
22. Redlich O, Kister AT (1948) *Ind Eng Chem* 40:345
23. Schmid-Fetzer RS, Gröbner J (2001) *Adv Eng Mater* 3:947
24. Servant C, Sundman B, Lyon O (2001) *Calphad* 25:79
25. Brillo J, Egry I (2007) *Int J Thermophys* 28:1004
26. Nowak R, Lanata T, Sobczak N, Ricci E, Giuranno D, Novakovic R, Holland-Moritz D, Egry I (2010) *J Mater Sci* 45:1993. doi:[10.1007/s10853-009-4061-z](https://doi.org/10.1007/s10853-009-4061-z)
27. Herlach DM, Cochrane RF, Egry I, Fecht HJ, Greer AL (1993) *Int J Mater Rev* 38:273
28. Paradis PF, Ishikawa T, Koike N (2006) *J Appl Phys* 100:103523
29. Krishnan S, Hansen GP, Hauge RH, Margrave JL (1990) *High Temp Sci* 29:17
30. Brillo J, Egry I, Ho I (2006) *Int J Thermophys* 27:494
31. Brillo J, Lohöfer G, Schmid-Hohagen F, Schneider S, Egry I (2006) *J Mater Prod Technol* 16:247
32. Cummings DL, Blackburn DA (1991) *J Fluid Mech* 224:395
33. Witusiewicz VT, Hecht U, Fries SG, Rex S (2004) *J Alloys Compd* 385:133
34. Witusiewicz VT, Hecht U, Fries SG, Rex S (2004) *J Alloys Compd* 387:217
35. Mills KC (2002) Recommended values of thermophysical properties for selected commercial alloys. Woodhead Publishing Ltd, Cambridge
36. Mills KC, Su YC (2006) *Int Mat Rev* 51:329
37. Keene B (1993) *Int Mater Rev* 38:157
38. Lee J, Shimoda W, Tanaka T (2004) *Mater Trans* 45:2864